

Anisotropy effects in a mixed quantum-classical Heisenberg model in two dimensions

C. Meyers, Y. Meurdesoif and Y. Leroyer,
Centre de Physique Théorique et de Modélisation de Bordeaux
Université Bordeaux I, CNRS, Unité Associée 1537
19 rue du Solarium, 33174 Gradignan Cedex, France
 and

O. Kahn
Laboratoire des Sciences Moléculaires
Institut de Chimie de la Matière Condensée de Bordeaux
CNRS, UPR 9048
Avenue Albert Schweitzer, 33608 Pessac Cedex, France
 (24/06/97)

We analyse a specific two dimensional mixed spin Heisenberg model with exchange anisotropy, by means of high temperature expansions and Monte Carlo simulations. The goal is to describe the magnetic properties of the compound $(\text{NBu}_4)_2\text{Mn}_2[\text{Cu}(\text{opba})]_3 \cdot 6\text{DMSO} \cdot \text{H}_2\text{O}$ which exhibits a ferromagnetic transition at $T_c = 15\text{K}$. Extrapolating our analysis on the basis of renormalisation group arguments, we find that this transition may result from a very weak anisotropy effect.

I. INTRODUCTION.

In the last few years there has been increasing interest in magnetic systems of low dimensionality. For example, the rapidly developing field of molecular magnetism [1] deals mainly with quasi one-dimensional and quasi two-dimensional compounds. Although the basic theory of their magnetic properties has been known for a long time [2] it is now necessary to apply it to the various contexts corresponding to these complex molecular architectures.

The compound $(\text{NBu}_4)_2\text{Mn}_2[\text{Cu}(\text{opba})]_3 \cdot 6\text{DMSO} \cdot \text{H}_2\text{O}$, synthesized by H.O. Stumpf *et al* [3], exhibits a transition at $T_c = 15\text{K}$ towards a ferromagnetically ordered state. The structure of this material can be schematically described by a superposition of negatively charged layers of hexagonal lattices with the Mn^{II} ions (spin 5/2) occupying the vertices and the Cu^{II} ions (spin 1/2) occupying the middle of the links (see figure 1). The tetrabutylammonium cations, NBu_4^+ , are located between the layers. Other compounds of the same kind have been synthesized, differing by the nature of the cations between the layers [4]. When these cations are small, (Na^+ , K^+ and tetramethylammonium) a long range antiferromagnetic ordering is observed in zero field. An external field of the order of 0.15 kOe is sufficient to overcome the very weak interlayer interactions and to lead to a ferromagnetic-like state. The compounds then behave as metamagnets. When the cations are larger (tetraethylammonium and beyond), a ferromagnetic ordering occurs at a critical temperature T_c . The value of this critical temperature first remains constant and equal to 15K, then decreases very smoothly as the cation size increases. In other respects, replacing Mn^{II} by a more anisotropic spin carrier such as Co^{II} results in a significant increase of T_c . These results suggest that both interlayer interactions and spin anisotropy are involved in the mechanism of long range ordering. The role of the spin anisotropy in the magnetic properties of two-dimensional compounds is much less documented than the three dimensional effects, and the goal of this paper is to address this problem.

In the layer of $(\text{NBu}_4)_2\text{Mn}_2[\text{Cu}(\text{opba})]_3 \cdot 6\text{DMSO} \cdot \text{H}_2\text{O}$, the nearest neighbour Mn^{II} and Cu^{II} ions interact through an antiferromagnetic coupling. The interlayer interaction in any case is very small as compared to the intralayer one, so that, to a good approximation, the spin system can be considered two-dimensional. In a previous paper [5], we have shown that such a simple description, in which the 5/2 spins Mn^{II} spins are approximated by classical ones, gives a good account of the magnetic and thermal properties of the paramagnetic phase of the compound. However, since the isotropic $O(3)$ model is critical only at zero temperature [6] we must include a symmetry breaking mechanism in order to explain the phase transition at $T_c = 15\text{K}$. We attribute this symmetry breaking to the presence of spin anisotropy.

Since no single crystal of the Cu-Mn compound has been obtained so far, a direct measurement of the orientation of the anisotropy is not possible. However, the existence of a spontaneous magnetization below T_c is the signal of an axial anisotropy and of an Ising-like transition. An in-plane anisotropy would have driven the system to be described

⁰CPTMB-97-9

by an XY symmetric model, which, in two dimensions, exhibits a Kosterlitz-Thouless transition with no ordered phase [7].

The aim of this paper, is to investigate the effect of a small axial anisotropy in the simple model described above.

For weak anisotropy, the critical properties of the model are dominated by the cross-over between the $T = 0$ critical point of the 2D Heisenberg model and the Ising one at T_c . This effect has been widely analysed in the framework of the purely classical Heisenberg model [8,9,10,11,12,13]. In particular, the renormalisation group analysis [11] leads to the following result : if λ is the anisotropy parameter ($\lambda = 0$ corresponds to the isotropic case) the Ising critical temperature decreases to zero as

$$T_c(\lambda) \approx \frac{1}{|\ln \lambda|} \quad \text{for } \lambda \rightarrow 0 \quad (1)$$

Furthermore, the zero-field susceptibility satisfies a scaling law

$$\chi(\lambda, T) = \chi(0, T) \Phi(\lambda e^{\frac{4\pi}{T}}) \quad (2)$$

where the function $\Phi(x) \approx |x - x_c|^{-7/4}$ for $x \approx x_c = \lambda e^{\frac{4\pi}{T_c}}$. This equation gives additional information on the Ising critical region. Let us define the width of this region, δ , by

$$1 - \delta \leq \frac{T}{T_c} \leq 1 + \delta \implies \chi(\lambda, T) \gg \chi(\lambda = 0, T)$$

From eq.(2) we get $\delta \approx \frac{1}{|\ln \lambda|}$ when $\lambda \rightarrow 0$. Therefore in the weak anisotropy limit we expect the Ising critical region to become very narrow and quite close to $T = 0$. Clearly, this makes experimental investigation difficult.

On the basis of universality, we transpose these renormalisation group results to our mixed spins system. Since we expect the anisotropy to be very small, we need to develop methods specifically designed to handle this cross-over effect. In section II we present our techniques of high temperature expansions on the one hand and of Monte-Carlo simulations on the other hand. In section III we analyse our results and, from a comparison with the experimental data, we determine the value of the anisotropy for the Cu-Mn compound. Conclusions are drawn in the last section.

II. THE MODEL.

We denote by $\mathbf{S}_j^{(\text{Mn})}$ the spin $\frac{5}{2}$ operator associated with the Mn ion at site j , and by $\mathbf{S}_i^{(\text{Cu})}$ the spin $\frac{1}{2}$ operator corresponding to the Cu ion at site i in the middle of a link of the honeycomb lattice. The antiferromagnetic interaction is represented by the Heisenberg hamiltonian

$$\mathcal{H} = J \sum_{\langle i,j \rangle} \left(\mathbf{S}_i^{(\text{Cu})} \cdot \mathbf{S}_j^{(\text{Mn})} + \lambda S_i^{z(\text{Cu})} S_j^{z(\text{Mn})} \right) - \left(\sum_{j=1}^{N_S} g_1 \mu_B \mathbf{S}_j^{(\text{Mn})} + \sum_{i=1}^{N_L} g_2 \mu_B \mathbf{S}_i^{(\text{Cu})} \right) \cdot \mathbf{H} \quad (3)$$

where J is positive, $\lambda (> 0)$ is the anisotropy parameter, \mathbf{H} is the external magnetic field, $\langle i, j \rangle$ stands for a pair of nearest neighbour spins, N_S is the number of sites and N_L is the number of links on the honeycomb lattice ($N_L = 3/2 N_S$). The spin $\frac{5}{2}$ operator can be approximated by a *classical* spin $S \mathbf{s}$ where \mathbf{s} is a unit classical vector and $S = \sqrt{\frac{5}{2}(\frac{5}{2} + 1)}$, whereas the spin $\frac{1}{2}$ operators are expressed in terms of the Pauli matrices, $\mathbf{S}^{(\text{Cu})} = \frac{1}{2} \sigma$. Since the quantum spin sites are not directly coupled to each other, one can trace out the quantum spin dependence to get a completely classical partition function

$$Z(T, \mathbf{H}) = \int \left(\prod_{i=1}^{N_S} d\Omega_i \right) \left\{ \prod_{\langle ij \rangle} 2 \cosh \left\| \mathbf{W}_{ij} + \frac{1}{2} \beta g_2 \mu_B \mathbf{H} \right\| \right\} \exp \left(\beta g_1 \mu_B S \mathbf{H} \cdot \sum_{i=1}^{N_S} \mathbf{s}_i \right) \quad (4)$$

where we have defined

$$\mathbf{W}_{ij} = -\frac{1}{2} \beta J S (\mathbf{s}_i + \mathbf{s}_j + \lambda (s_i^z + s_j^z) \hat{\mathbf{e}}_z) \quad (5)$$

and $\|\mathbf{X}\|$ stands for the length of the vector \mathbf{X} . The indices i and j now label the *classical* spins located at the vertices of the honeycomb lattice.

By choosing the orientation of the magnetic field parallel to the anisotropy axis, or orthogonal to it (along the x axis), we define $Z_\mu(T, H) \equiv Z(T, H \hat{\mathbf{e}}_\mu)$ with $\mu = x$ or z , as follows :

$$Z_\mu(T, H) = \int \left(\prod_{i=1}^{N_S} d\Omega_i \right) \left\{ \prod_{\langle ij \rangle} 2 \cosh (K \phi_{\langle ij \rangle}^\mu) \right\} \exp \left(\beta g_1 \mu_B S H \sum_{i=1}^{N_S} s_i^\mu \right) \quad \mu = x \text{ or } z \quad (6)$$

with $K = \frac{1}{2} \beta J S$ and $\phi_{\langle ij \rangle}^\mu = \|\mathbf{s}_i + \mathbf{s}_j + \lambda(s_i^z + s_j^z) \hat{\mathbf{e}}_z - \frac{g_2 \mu_B}{J S} H \hat{\mathbf{e}}_\mu\|$

We shall be interested in the standard observables : the specific heat $C_V = k_B T^2 \frac{\partial^2}{\partial T^2} \ln Z(T, 0)$, the susceptibility along the different directions $\chi_\mu = \frac{k_B T}{V} \frac{\partial^2}{\partial H^2} \ln Z_\mu \Big|_{H=0}$, and the total susceptibility, $\chi = \frac{1}{3} \chi_z + \frac{2}{3} \chi_x$, which is measured experimentally

III. THE METHOD OF ANALYSIS

A. The high temperature expansion.

We have performed the expansion of $\ln Z_\mu$ in power series of K up to the 19th order and to the second order in H for computing the magnetic susceptibility. Then we analysed the series for decreasing values of the anisotropy parameter. The complexity of the nearest neighbour interaction (eq.(6)) does not allow the standard techniques [8,14,15] to be used.

The diagrammatic expansion is generated by replacing in eq.(6) each $\cosh (K \phi_{\langle ij \rangle}^\mu)$ term by $1 + \Psi_{\langle ij \rangle}^\mu$ where the function $\Psi_{\langle ij \rangle}^\mu$ results from the expansion of the hyperbolic cosine in power series of K to the given maximal order and of H to the second order. To each function $\Psi_{\langle ij \rangle}^\mu$ appearing in the product over the nearest neighbour pairs in eq.(6), is associated one link of a graph G . In this way, a link contains all positive powers of K .

The powerful star graph expansion technique [15] cannot be used here since, due to the presence of the anisotropy term, the partition function of articulated graphs does not factorise. Our procedure is based on the the standard connected graph expansion [15] for the normalised partition function $\tilde{Z}_\mu = Z_\mu(T, H) / Z_\mu(T, H)|_{J=0}$

$$\ln \tilde{Z}_\mu(T, H) = \sum_{\{G\}} C(G) \omega(G)$$

where $\{G\}$ is the set of all connected graphs to a given order, $C(G)$ the embedding constants of the graph G , and $\omega(G)$ its weight. The weights $\omega(G)$ are constructed through the recursive technique $\ln \tilde{Z}_\mu(G) = \sum_{\{g\}} \omega(g)$, where $\{g\}$ is the set of all subgraphs of G .

The main difficulty of the method resides in the computation of $\ln \tilde{Z}_\mu(G)$, given by :

$$\ln \tilde{Z}_\mu(G) = \int \left(\prod_{i \in G} d\Omega_i \right) \left(\prod_{\ell \in G} \Psi_\ell^\mu \right) \exp \left(\beta g_1 \mu_B S H \sum_{i \in G} s_i^\mu \right) \quad (7)$$

where $\{\ell\}$ and $\{i\}$ are respectively the set of links and of vertices belonging to the graph G . We proceed as follows :

- (a) By using the spherical harmonic basis and the reduction formula, each function $\Psi_{\langle ij \rangle}^\mu$ can be expressed as :

$$\Psi_{\langle ij \rangle}^\mu = \sum_{l_1 m_1 l_2 m_2} \Lambda_{l_1 m_1}^{l_2 m_2} Y_{l_1 m_1}(\Omega_i) Y_{l_2 m_2}(\Omega_j)$$

where $\Lambda_{l_1 m_1}^{l_2 m_2}$ is a matrix built recursively of which elements are power series in K and H .

- (b) The exponential term in eq.(7) is expanded to second order in H , and the spin dependence expressed in terms of the spherical harmonics.
- (c) The integral is then computed, contracting the products of spherical harmonics by means of the reduction formula, and then integrating over the residual angular variables.

As an illustration of our results, we give in table I the coefficients of the development of χ_z to the zeroth and first order in λ .

The series for the zero-field susceptibility is then analysed by means of the Padé extrapolation technique. For our system, the renormalisation group result of eq.(2) becomes [5] :

$$\frac{\chi(\lambda, K)}{\chi(0, K)} = \Phi(\lambda e^{\frac{2\pi}{\sqrt{3}}K}) \quad \text{with } K = \frac{1}{2}\beta JS \quad (8)$$

where the function $\Phi(x) \approx |x - x_c|^{-7/4}$ for $x \approx x_c = \lambda e^{\frac{2\pi}{\sqrt{3}}K_c}$. For small λ , the singularity is located at large values of K , far away from the perturbative region. According to these results, we analysed the function $\left(\frac{\chi(\lambda, K)}{\chi(0, K)}\right)^{4/7}$ in terms of the variable $v = 1 - e^{-\alpha K}$, small at high temperature but bounded for large K . The variational parameter α is optimised by stabilising the Padé table. For very low values of λ the determination of the critical temperature resulting from the location of the poles becomes inaccurate giving large error bars. For $\lambda \lesssim 10^{-2}$ an extension of the series to higher orders is needed to reliably get precise results from this method. However, in this very weak regime of anisotropy, once the critical temperature is known by another method - Monte-Carlo simulation for instance - the series becomes a useful analytic representation of the observables. It will be used to determine the physical parameters from a comparison with the experimental data.

The results of this analysis will be presented and discussed in the next section together with the Monte-Carlo results.

B. The Monte-Carlo simulation.

We performed a Monte Carlo simulation in order to verify the results of the high temperature expansion, and to investigate the very small anisotropy regime where the perturbative technique fails. The simulation is based on the effective classical model

$$-\beta\mathcal{H}_{\text{eff}} = \sum_{\langle ij \rangle} \ln(2 \cosh \|\mathbf{W}_{ij}\|) \quad (9)$$

where \mathbf{W}_{ij} is defined in eq.(5). The various observables can be expressed as ensemble averages with respect to the Boltzmann weight $e^{-\beta \mathcal{H}_{\text{eff}}} / Z(T, 0)$. Their expression is a simple generalisation of the definition of eqs.(6,8) of ref. [5] in which W_{ij} is replaced by the new definition of eq.(5).

Our goal is to explore the weak anisotropy regime where the cross over effect between the 2D Heisenberg and Ising fixed points is important. As the anisotropy gets smaller, most of the low temperature region is dominated by the 2D Heisenberg regime in which the correlation length remains large due to the essential singularity at $T = 0$. Therefore, the usual limitations of the Monte-Carlo procedure - critical slowing down and the finite size effects - constrain rather severely the simulation of these systems.

In order to overcome the first problem we used a global algorithm. We have adapted the Wolf algorithm [16] to the case of an anisotropic interaction. The 'Ising' orientation of the spins, used to construct the Wolf cluster and which is randomly chosen in the standard algorithm, is imposed here by the anisotropy. In our procedure, a Monte-Carlo update proceeds in three steps :

1. construct a first cluster with respect to the z (anisotropy) axis and flip the corresponding spin components ;
2. construct another cluster relative to a randomly chosen direction in the $x - y$ plane and flip the corresponding spin components ;

After these two steps, a given spin remains on the cone defined by its initial orientation and the z -axis. Therefore we proceed to another step :

3. change the actual orientation of each spin of the lattice according to a standard Metropolis algorithm. This operation is repeated twice.

We checked that this procedure allows us to recover the results of the zero-anisotropy case [5], and of the strong anisotropy (classical Ising) limit with a very small critical slowing down effect.

The second problem concerns the finite size effects. For small λ , since we investigate the low temperature region where the correlation length remains large even outside the Ising critical region, we need large lattices. We have limited our analysis to $\lambda = 0.001$, and to a maximum lattice size of $L = 256$.

IV. RESULTS

A. The critical temperature.

To validate our methods we compare the results obtained by both procedures. We present in figure 2 the zero-field susceptibility, orthogonal to the anisotropy axis (χ_x) and parallel to it (χ_z) for the high temperature series and the Monte-Carlo data as a function of K and for a moderately small value of the anisotropy parameter $\lambda = 0.1$. The agreement between these two results is very good. These curves clearly show the divergent behaviour of the axial susceptibility, which will be used to determine the critical temperature in the Monte-Carlo simulation. Figure 3 displays the specific heat as a function of K for the same anisotropy. Besides the good agreement between the two methods, we observe the clear critical signal at $K_c \simeq 2.21$ which emerges from the comparison with the result for the isotropic model.

The critical temperature is obtained from the Monte-Carlo data by localising the peak in the specific heat and the inflexion point of the susceptibility as a function of the temperature. In order to estimate the precision of such a determination we performed a complete finite size scaling analysis of the data at $\lambda = 0.1$ to obtain the critical temperature and the susceptibility exponent. The results are presented in figure 4 where we plotted $T_c(L)$, measured from the two signals, for several lattice sizes (fig.(4a)), and in fig.(4b) $\ln \chi$ as a function of $\ln |K_c - K|$. Fig.(4a) shows a small variation of the finite system critical signal, which allows us to estimate the bulk critical temperature T_c from lattices of size not exceeding $L = 128$. With this estimate, we determine the exponent γ of the susceptibility from fig.(4b). The result $\gamma = 1.74(2)$ is in very good agreement with the expected exact Ising value $\gamma = 1.75$. This is a self-consistent indication of the reliability of the critical temperature measurement. Furthermore, we check that the Monte-Carlo result falls inside the error bar obtained from the high temperature series analysis.

With this method, we determined the critical coupling $K_c = \frac{1}{2} \frac{JS}{k_B T_c}$ as a function of the anisotropy parameter on lattices of size $L \leq 256$ down to $\lambda = 0.001$. The results of both analyses - Monte-Carlo and high temperature expansion - are displayed in figure 5. Fig.(5a) shows the general trend of the variations of $K_c^{-1} \propto T_c$ as a function of λ , with a decrease to zero for $\lambda \rightarrow 0$, and a linear variation at large λ . Actually, for $\lambda \rightarrow \infty$, the model coincides with a classical Ising model with coupling $K_{\text{Ising}} = \lambda K$ so that, in this limit, $K_c^{-1}(\lambda) \simeq \lambda K_c^{-1} \text{Ising}$. From the high temperature expansion, we get the estimation $K_c \text{Ising} \simeq 1.46(1)$. The variations for small λ are presented in fig.(5b) where we plotted K_c vs $\ln \lambda$. It appears that the behaviour predicted by the renormalisation group (eq.(1)) is obtained for very small anisotropy. Actually, from fig.(5b) we obtain :

$$K_c = \frac{\sqrt{3}}{2\pi} |\ln \lambda| + 2.41 \quad \lambda \lesssim 0.001. \quad (10a)$$

Therefore, by extrapolating this behaviour down to $\lambda \rightarrow 0$, we are able to predict the critical temperature for very small anisotropy.

B. Comparison with the experimental results.

In order to compare with the experimental results, we proceed in two steps.

- We get an estimation of the anisotropy parameter from the value of J previously determined in the analysis of the paramagnetic phase [5] and from the experimental critical temperature $T_c = 15$ K. We obtain $K_c \simeq 4.6$ which corresponds to $\lambda \simeq .0004$, according to the fig.(5b).
- We perform an adjustment of J , g_1 and g_2 at fixed λ by fitting the experimental data with a selected Padé approximant. Small variations around the fixed λ value do not significantly change the fit.

The results are presented in figure 6, for the whole range of temperature in fig.(6a) and for the critical region only in fig.(6b). An excellent agreement with the experimental data is obtained with the following set of parameters :

$$J = 45.5 \text{ K} \quad , \quad g_1 = 2.0 \quad , \quad g_2 = 2.11 \quad , \quad \lambda \simeq .0005$$

The exponential variation of λ with respect to T_c (eq.(10a)) induces rather large error bar on the determination of λ : actually, an error of one kelvin on T_c induces a variation of λ by a factor of 3. However, the magnetic susceptibility is rather insensitive to these variations which only affect the Ising critical region, in such a narrow range of temperature that it is not visible experimentally. Moreover, the high temperature ($T \geq 50$ K) behaviour is left completely unchanged by such a small perturbation, thus preserving the good agreement with the isotropic model observed in ref. ([5]).

V. CONCLUSIONS

We have determined the spin anisotropy which is present in the Cu-Mn magnetic compound [3] and which is responsible for a ferromagnetic transition at 15K. Two methods are used in a complementary way, high temperature expansion and Monte-Carlo simulation, in order to extract reliable results out of the strong cross-over regime where the effect lies. Assuming universality and extending the renormalisation group results to our situation, we obtain a very small value for the anisotropy parameter.

The strong behaviour $T_c(\lambda) \approx \frac{1}{|\ln \lambda|}$ is responsible for the fact that a very weak perturbation ($\lambda \simeq 10^{-4}$) produces a sizeable effect ($T_c \simeq 15$ K). For these quasi-two dimensional molecular compounds, involving high spin magnetic ions, it is unconceivable that at such a low level of magnitude the anisotropy is absent. Therefore we should always expect a ferromagnetic transition at an appreciable critical temperature in these systems.

In this work, we only considered the exchange anisotropy as a source of the O(3) symmetry breaking. Alternatively, the on site anisotropy could be present, but in the limit of weak anisotropy under consideration here, on the ground of universality we expect the results to be unchanged. Concerning the interlayer interactions which have been neglected in our approach, it is known [12] that if the ratio of the interlayer to the intralayer coupling, $\sigma = \frac{J_{\parallel}}{J_{\perp}}$, is small, the transition temperature induced by these three dimensional effects behaves like $T_c \approx \frac{1}{\ln|\sigma|}$. Therefore, even a very small interplane coupling may significantly contribute to the measured critical temperature, in competition with the anisotropy effect. We have seen that increasing the interlayer distance beyond a certain limit results in a smooth decrease of T_c . Taking into account the interlayer coupling would require to introduce an additional cross-over effect between the three dimensional model with spatial anisotropy and the two dimensional one with exchange anisotropy [12]. As a consequence, the contribution of the spin anisotropy to the critical temperature would be overestimated and our result for the anisotropy parameter would turn out to be an upper bound.

Acknowledgements

We thank S.V. Meshkov for his contribution to the Monte-Carlo part of this work and J. Leandri for helpful discussions.

-
- [1] O. Kahn, *Molecular Magnetism*, VCH Publisher, New-York 1993
 - [2] W. Heisenberg, *Z.Physik* **49**, (1928) 619
 - [3] H.O. Stumpf, Yu Pei, O. Kahn, J. Sletten and J.P. Renard, *J. Am. Chem. Soc.* **115**, (1993) 6738
 - [4] O. Cador, D. Price, J. Larionova, C. Mathonière, O. Kahn, J.V. Yakhmi ; to be published in *J. Mater. Chem* **7** (1997)
 - [5] J. Leandri, Y. Leroyer, SV Meshkov, Y Meurdesoif, O Kahn, B Mombelli and D. Price, *J. Phys. C* **8** (1996) L271
 - [6] N. D. Mermin and H. Wagner, *Phys. Rev. Lett.* **17**, (1966) 1133
 - [7] J.M. Kosterlitz and D.J. Thouless, *J. Phys. C* **6** (1973) 1181
 - [8] D. Jasnow and M. Wortis, *Phys. Rev.* **176**, (1968) 739
 - [9] P. Pfeuty, D. Jasnow and M.E. Fisher, *Phys. Rev.* **B10**, (1974) 2088
 - [10] K. Binder and D.P. Landau, *Phys. Rev.* **B13**, (1976) 1140
 - [11] R.A.Pelcovits and D.R.Nelson, *Phys. Lett.* **A57**, (1976) 23 ; D.R.Nelson and R.A.Pelcovits, *Phys. Rev.* **B16**, (1977) 2191
 - [12] S. Hikami and T. Tsuneto, *Prog. Theor. Phys.* **63**, (1979) 387
 - [13] A. Cuccoli, V. Tognetti and R. Vaia, *Phys. Rev.* **B52**, (1995) 10221
 - [14] G.S. Rushbrooke, G.A.Baker and P.J. Wood in "Phase transitions and critical phenomena", vol. 3, p. 246, C. Domb and M.S. Green editors, (Academic Press, 1974)
 - [15] S. McKenzie, *NATO advanced Study Series : Phase Transitions* **B72**, (1980) 271
 - [16] U. Wolf, *Phys. Rev. Lett.* **62**, (1989) 361 and *Nucl. Phys.* **B344** (1990) 581

	λ^0		λ^1	
	$S^2 g_1^2$	g_2^2	$S^2 g_1^2$	g_2^2
K^0	$\frac{2}{9}$	$\frac{1}{4}$	0	0
K^2	$\frac{2}{9}$	$\frac{2}{9}$	$\frac{28}{45}$	$\frac{2}{3}$
K^4	0	$-\frac{1}{15}$	$\frac{32}{81}$	$\frac{6}{25}$
K^6	$\frac{2}{225}$	$\frac{533}{8505}$	$\frac{1532}{30375}$	$\frac{5282}{42525}$
K^8	$-\frac{4}{2835}$	$-\frac{5683}{127575}$	$\frac{512}{14175}$	$-\frac{1754}{25515}$
K^{10}	$\frac{524}{893025}$	$\frac{19912}{601425}$	$-\frac{128824}{9568125}$	$\frac{219628}{2525985}$
K^{12}	$-\frac{69464}{35083125}$	$-\frac{51038503}{1915538625}$	$\frac{117344}{526246875}$	$-\frac{14083390696}{143665396875}$
K^{14}	$\frac{4539614}{1149323175}$	$\frac{6380434}{273648375}$	$\frac{5687869652}{430996190625}$	$\frac{20243410804}{184712653125}$
K^{16}	$-\frac{408296024}{86199238125}$	$-\frac{87518482699}{4396161144375}$	$-\frac{62768262944}{4114054546875}$	$-\frac{3168011262218}{29973825984375}$

	λ^0	λ^1
	$S g_1 g_2$	$S g_1 g_2$
K^1	$-\frac{2}{3}$	$-\frac{2}{3}$
K^3	$-\frac{2}{27}$	$-\frac{166}{135}$
K^5	$-\frac{8}{405}$	$-\frac{152}{675}$
K^7	$\frac{2}{8505}$	$-\frac{69758}{637875}$
K^9	$-\frac{4}{4725}$	$\frac{44524}{1913625}$
K^{11}	$\frac{7108}{49116375}$	$-\frac{316875236}{11051184375}$
K^{13}	$\frac{45214696}{5746615875}$	$\frac{11621348744}{143665396875}$
K^{15}	$-\frac{2434334054}{86199238125}$	$-\frac{130568299906}{587722078125}$
K^{17}	$\frac{875743046944}{13987785459375}$	$\frac{419699964912544}{887686384921875}$

Table I : A subset of the coefficients of the high temperature series for the axial susceptibility χ_z in powers of $K = \frac{1}{2}\beta JS$ up to the 17th order. The coefficient of K^n is a polynomial of degree n in the anisotropy parameter λ . For each coefficient we only give the constant and linear term in λ (columns with heading λ^0 and λ^1 respectively)

The top half of the table contains the even power coefficients ; for each power of λ the fraction of the first sub-column must be multiplied by $S^2 g_1^2$ and added to the second multiplied by g_2^2 . For instance, the coefficient of K^2 is : $\frac{2}{9}S^2 g_1^2 + \frac{2}{9}g_2^2 + \lambda(\frac{28}{45}S^2 g_1^2 + \frac{2}{3}g_2^2) + O(\lambda^2)$

The bottom half of the table contains the odd power coefficients ; the fraction in each column must be multiplied by $S g_1 g_2$.

Figure Captions

Figure 1 : An elementary cell of the hexagonal lattice, with the Cu ions (closed circles) at the middle of the links and the Mn ions (open circles) at the vertices.

Figure 2 : The susceptibility multiplied by the temperature, as a function of the reduced coupling $K = \frac{1}{2}\beta JS$ for an anisotropy $\lambda = 0.1$. The data points come from the Monte-Carlo simulation ; the solid line corresponds to the Padé approximant of the high temperature expansion (H.T.E.).

(a) the in-plane susceptibility ;

(b) the axial susceptibility ; the closed circles correspond to a lattice size $L = 128$ and the triangles to $L = 256$.

Figure 3 : The specific heat as a function of K .

- for an anisotropy parameter $\lambda = 0.1$: the Monte-Carlo data are represented by the closed circles for a lattice size $L = 128$ and by open triangles for $L = 256$. The solid line corresponds to the high temperature expansion (Padé approximant).
- for the isotropic model ($\lambda = 0$) : the open circles correspond to the Monte-Carlo simulation ($L = 64$) and the dashed line to the series result..

Figure 4 Analysis of the Ising critical regime :

(a) The finite size critical temperature as a function of the lattice size L :

- from the maximum of the specific heat (triangles)
- from the inflexion point of the axial susceptibility (circles)

(b) the axial susceptibility as a function of $|K_c - K|$ in log-log scale. The slope of the fitted straight line is 1.74(2) in good agreement with the expected exact Ising value $\gamma = 1.75$.

Figure 5 Variation of the critical temperature with λ . The series results are represented by open circles and the Monte-Carlo simulation by closed circles.

(a) The large anisotropy regime : we plot the inverse of the reduced critical coupling $K_c^{-1} = \frac{2k_B T_c}{JS}$ as a function of the anisotropy parameter. The slope of the linear behaviour, expected at large λ corresponds to $K_c \text{ Ising} \simeq 1.46(1)$.

(b) The weak anisotropy regime : the reduced critical coupling K_c as a function of λ in a logarithmic scale. The solid line corresponds to the renormalisation group behaviour $K_c = -\frac{\sqrt{3}}{2\pi} \ln \lambda + \text{const}$. The value of the constant is 2.41(2).

Figure 6 Fit of the experimental data (closed circles for sample 1, open circles for sample 2) for the total magnetic susceptibility. The solid line corresponds to a Padé approximant of the high temperature series with the parameter : $J = 45.5$ K, $g_1 = 2.0$, $g_2 = 2.14$, $\lambda = .0005$;

(a) for the whole temperature range

(b) for the critical region. The difference between the two samples gives an estimation of the experimental errors in the critical region.

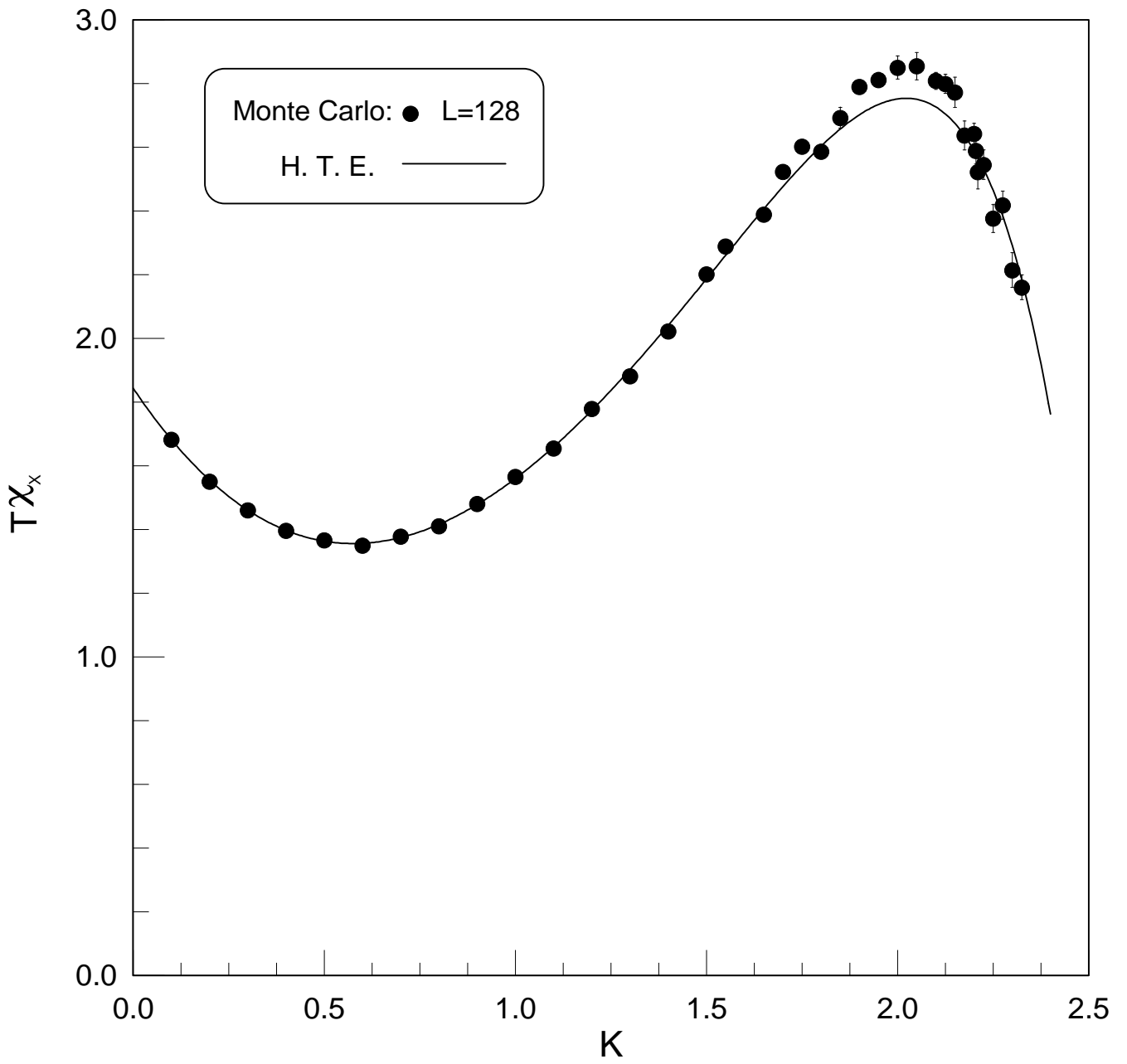


Figure 2 (a)

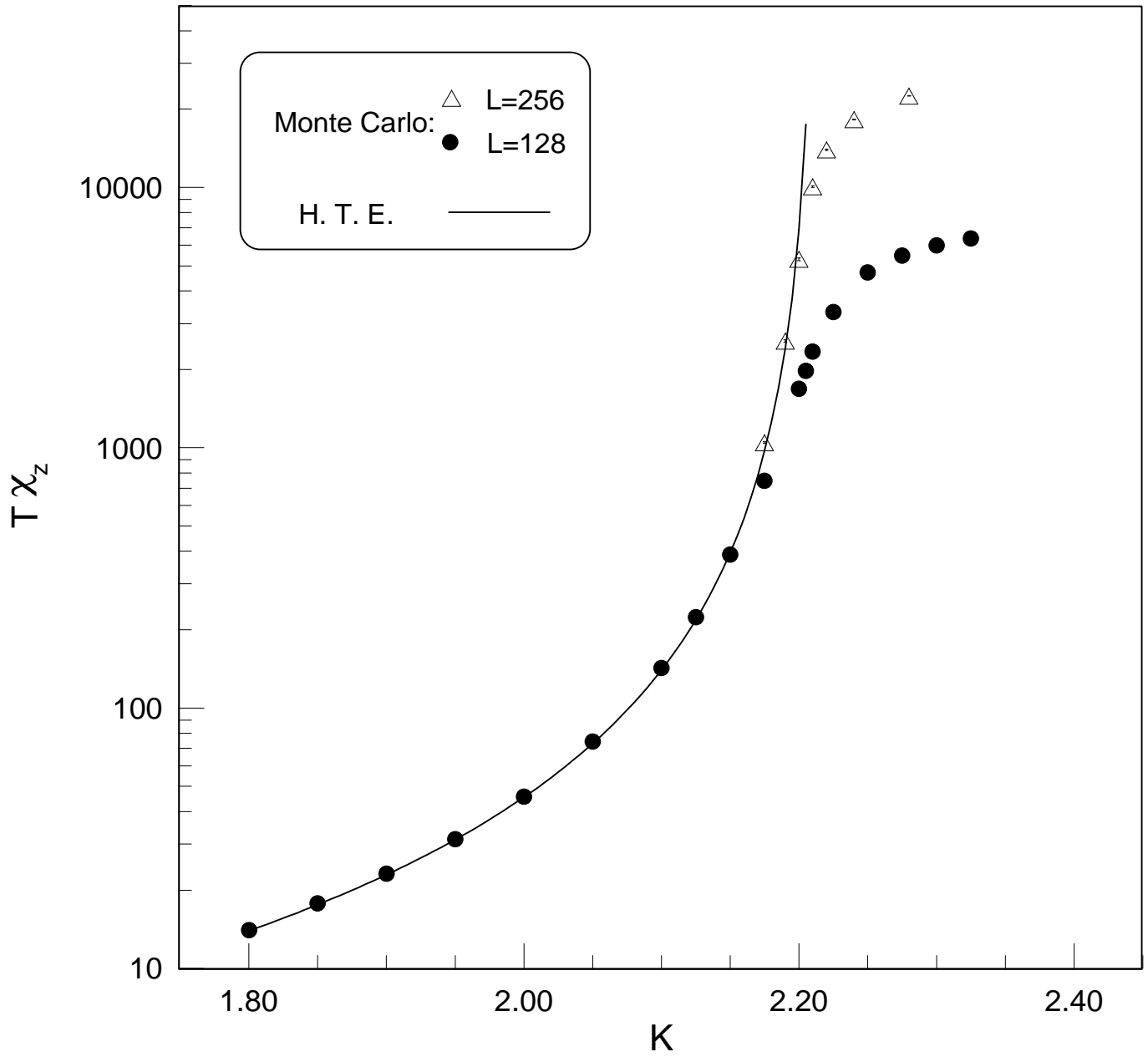


Figure 2 (b)

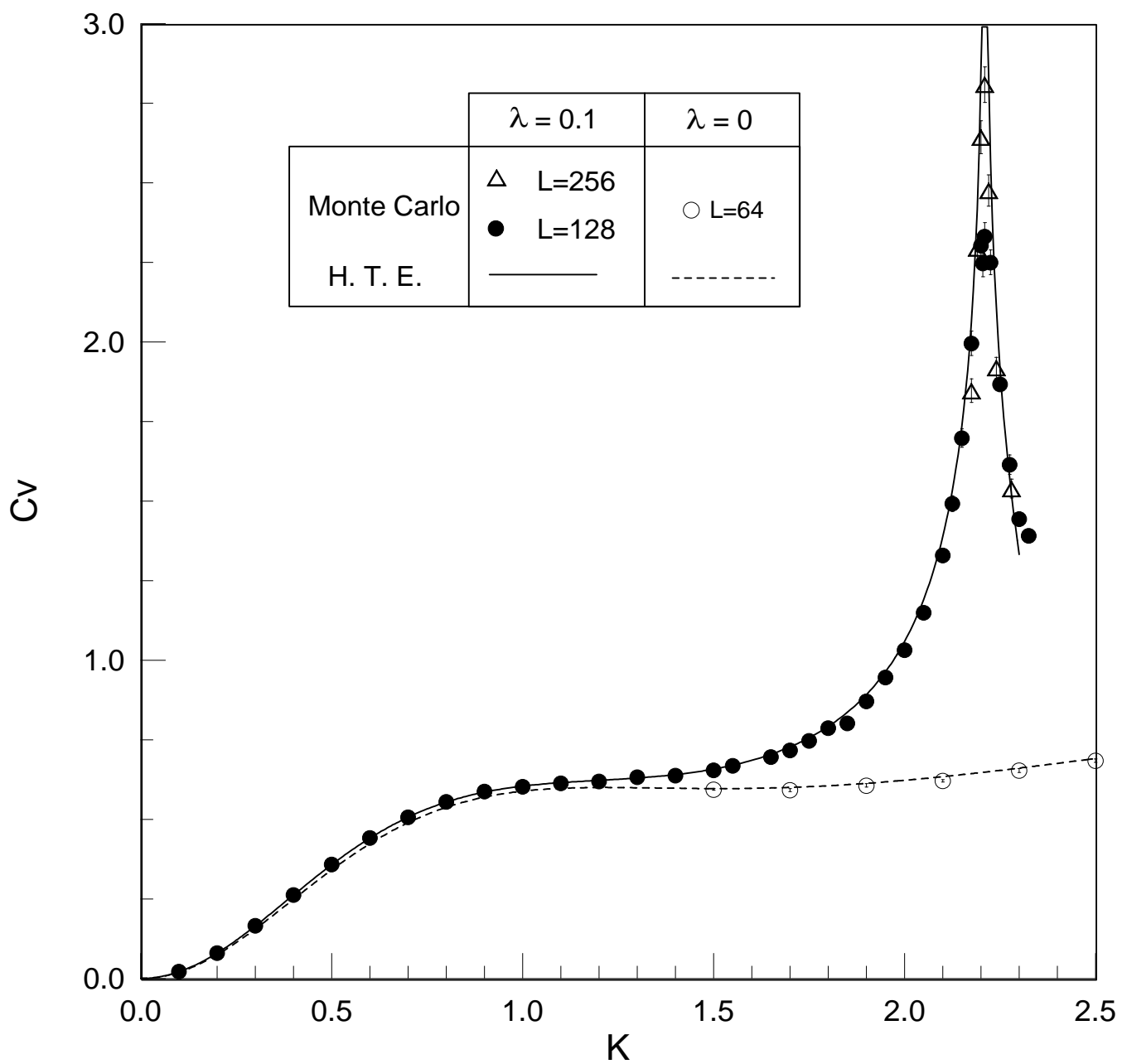


Figure 3

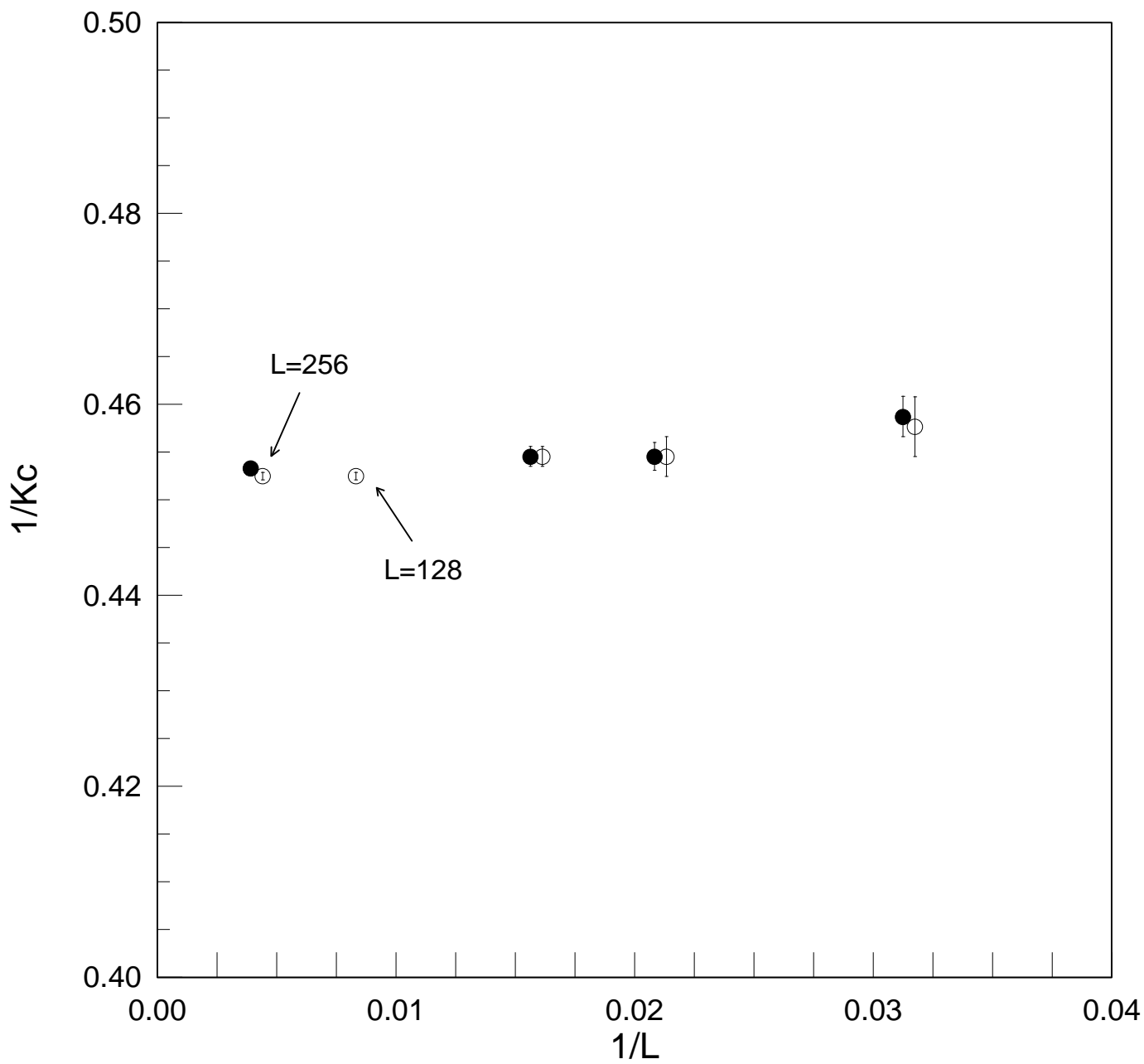


Figure 4 (a)

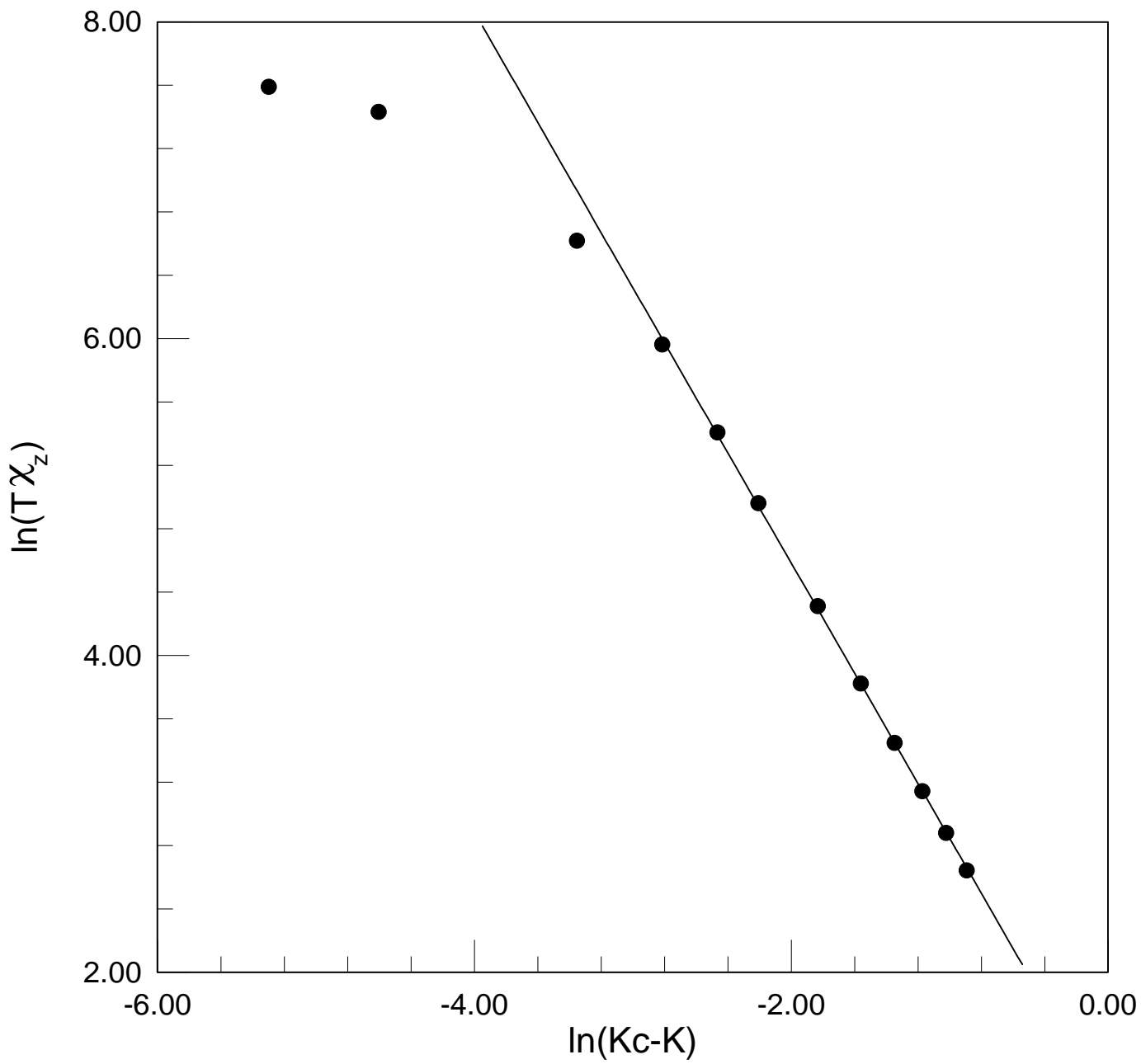


Figure 4 (b)

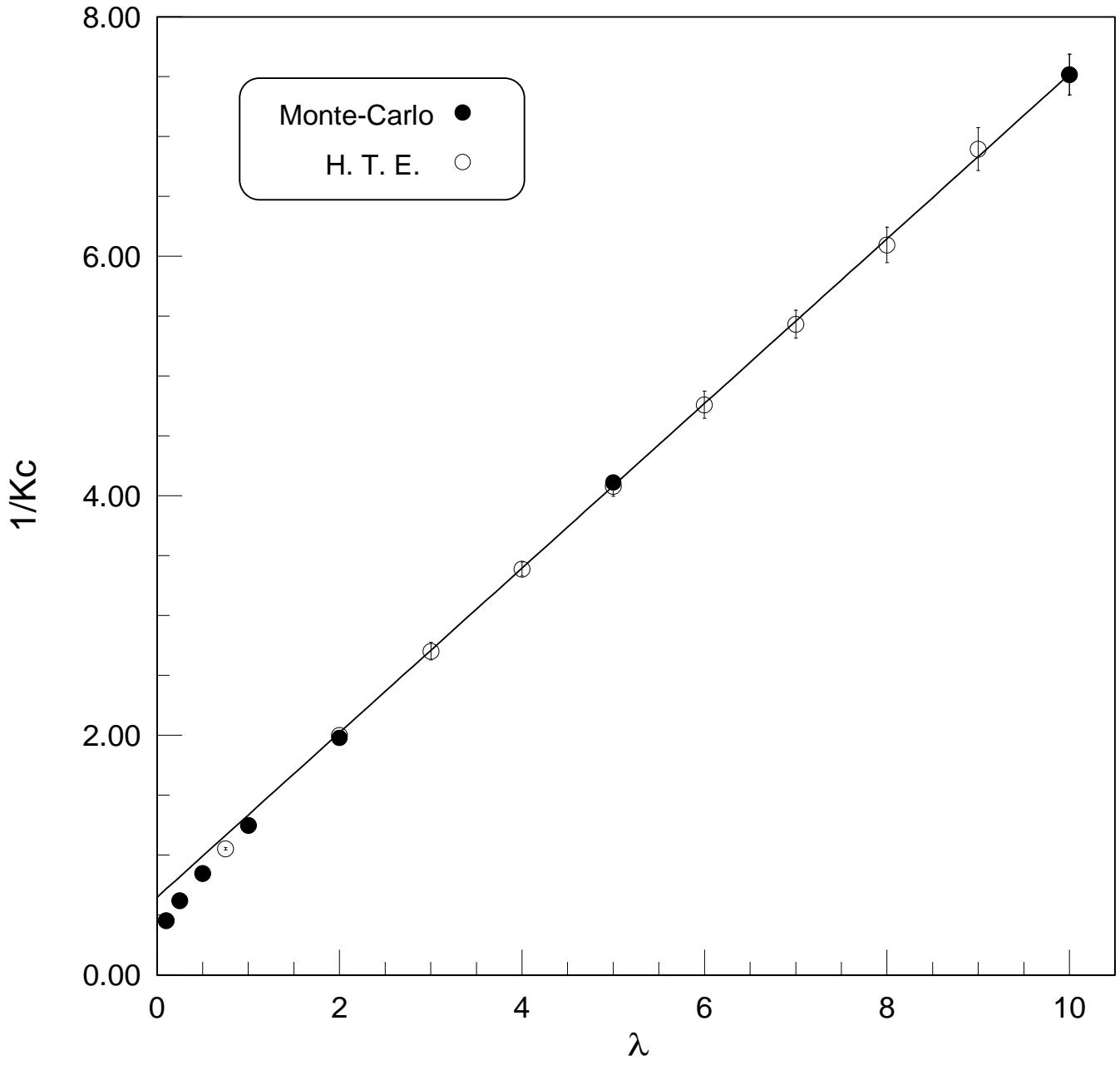


Figure 5 (a)

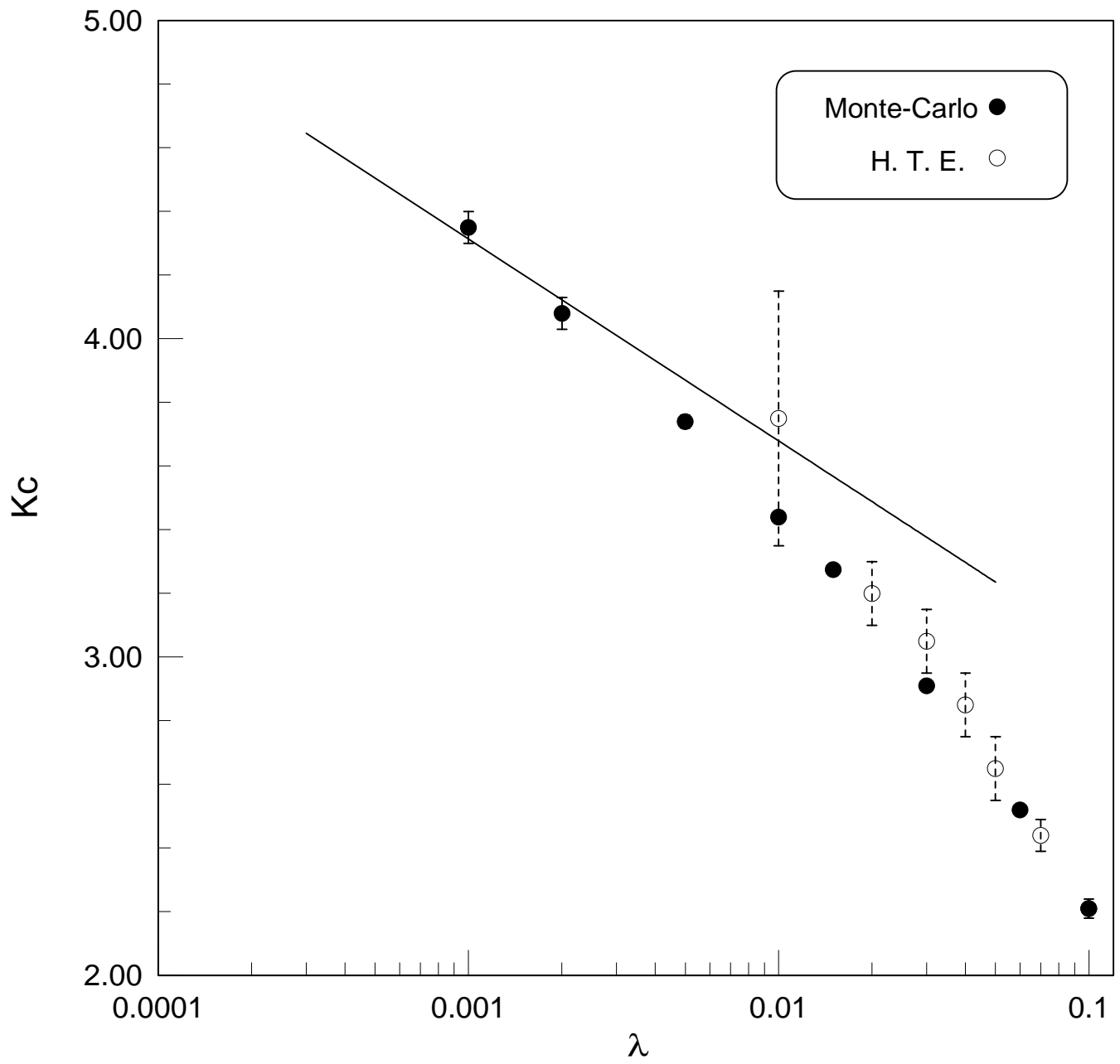


Figure 5 (b)

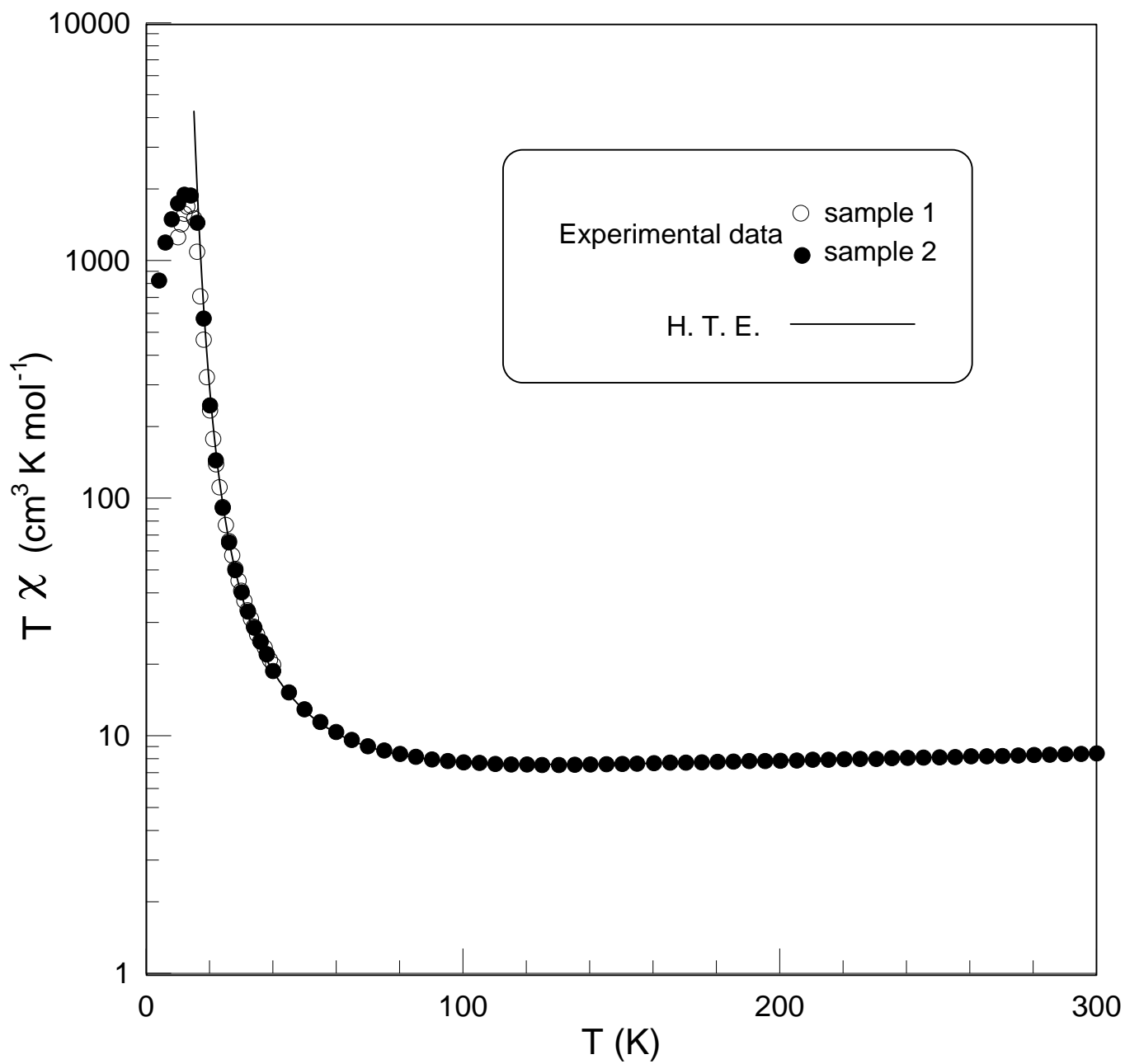


Figure 6 (a)

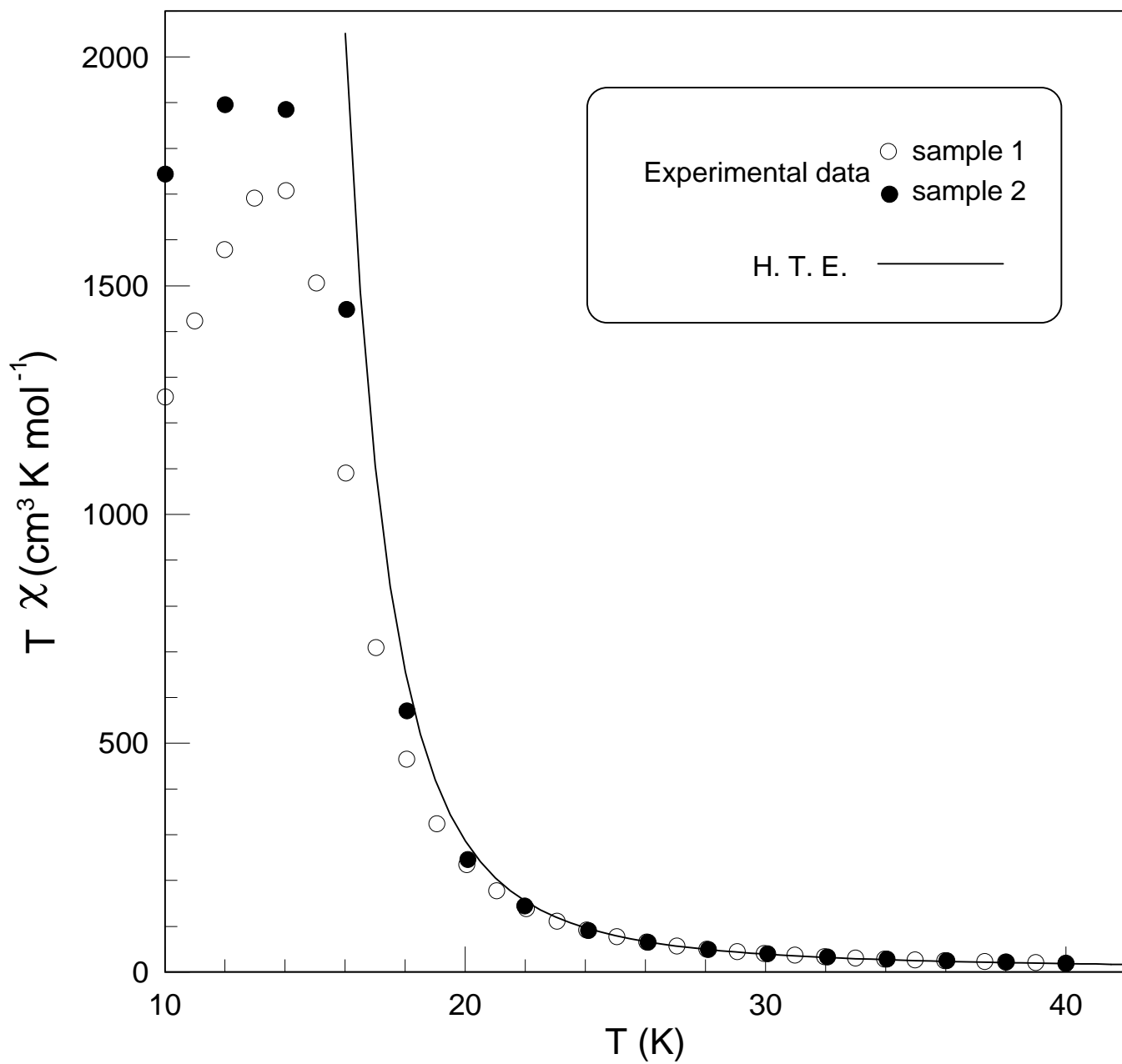


Figure 6 (b)